Internal mass transfer considerations in biofilms of succinic acid producing *Actinobacillus succinogenes*

Sekgetho Charles Mokwatlo[a], Willie Nicol[a], Hendrik Gideon Brink[a,*]

Department of Chemical Engineering, University of Pretoria, Lynnwood Road, Hatfield, 0002, Pretoria, South Africa

Highlights

•Internal mass transport considerations are critical in *A. succinogenes* biofilms.

•Internal mass transport governs long term stability and biofilm effectiveness.

•A simplified algorithm is presented to quantify steady state biofilm mass transport.

•Biofilm growth conditions proposed for optimal stability and effectiveness.

Postal address: Department of Chemical Engineering, University of Pretoria, Private Bag X20, Hatfield, 0028, South Africa

E-mail addresses:

Mr. S.C. Mokwatlo: u11119072@tuks.co.za

Prof. W. Nicol: willie.nicol@up.ac.za

* corresponding author: Dr H.G. Brink: deon.brink@up.ac.za

Abstract

The rumen bacterium *Actinobacillus succinogenes* is reputable for its high productivity, -yield and -titre fermentative production of succinic acid under biofilm conditions. The paper presents an analysis of internal mass transfer effects in biofilm fermentations of *A. succinogenes*. Internal mass transfer effects were investigated by batch fermentations using attached- and resuspended biofilms as biocatalysts. In the latter, the biofilms were resuspended after initial development to simulate mass transfer free (free cell) fermentations. Intrinsic kinetics for succinic production obtained from resuspended free cell fermentations predicted faster production rates than for the attached biofilms runs (biofilm thicknesses in the range of 120 – 200 μm), indicating internal mass transfer restrictions. A developed biofilm reaction diffusion model gave good predictions of attached biofilm batch results by accounting for internal mass transfer in the biofilm. Biofilm effectiveness factors ranged from 75% to 97% for all batches at the inception of batch conditions but increased with progression of batch operation due to increased succinic acid titres which inhibited production rates. Biofilm thickness and succinic acid concentrations were shown to have a significant effect on internal mass transfer. A simplified algorithm was developed to estimate the pseudo-steady state glucose penetration and biofilm effectiveness of *A. succinogenes* biofilms without the requirement to solve the overall mass transfer model. The results clearly showed that internal mass transfer need to be considered in biofilm fermentations involving *A succinogenes* as high biomass concentrations may not always equate to increased productivities if mass transfer effects dominate.

Keywords: *Actinobacillus succinogenes*; internal mass transfer; biofilm; succinic acid

1. Introduction

The bovine rumen bacterium *Actinobacillus succinogenes* has established itself as a promising microbial biocatalyst to produce succinic acid (SA) when compared to other recognized wild-type SA bio-producers [1–4]. These include microorganisms such as *Mannheimia succiniciproducens* [5], *Anaerobiospirillum succiniciproducens* [6], *Basfia succiniciproducens* [7], and modified strains of *Escherichia coli* [8]. Key among the traits that make *A. succinogenes* a desirable biocatalyst is the predictable establishment of biofilms during continuous fermentations [9,10]. Biofilm formation facilitates significantly higher cell densities than would be possible without active cell retention strategies and therefore realizes exceptional SA volumetric productivities and -titres. In addition, biofilms promote enhanced tolerance to toxic reagents and long-term activity; desirable qualities during continuous processing where stability is a requirement [9–12].

The microbial production of SA from renewable plant derived feedstocks has received considerable research interest in recent years. SA is a top biobased platform chemical which is punted to replace current petroleum-based feedstocks as a starting material for the synthesis of important commodity chemicals such as 1,4-butanediol, maleic anhydride, and adipic acid [13]. This would help, in part, to usher in a biomass dependent bioeconomy therefore attenuating the global reliance on harmful petroleum-based resources. Though commercial bio-production of SA has been implemented by several companies such as BioAmber, Reverdia, Myriant, and BASF-Purac, these facilities mostly cater of niche markets due to the high production costs. For SA to compete as a viable platform chemical requires production costs of circa 1 USD/kg SA. This implies that low capital outlay and operational expenses – the use of facultative anaerobes such as *A. succinogenes* avoid high aeration costs – and high throughput processes

are essential for long-term sustainability of these biopolymer and organosynthetic industries [14].

Unlike free cell fermentations, biofilm fermentations are prone to mass transfer limitation phenomena. Nutrients and substrates must diffuse within the biofilm matrix to be accessed by the biofilm cells [15]. Numerous biofilm fermentation studies on *A. succinogenes* include batch [16], fed batch [16], repeat batch [17], and continuous [9,10,17] bioreactor operation strategies. In most of these studies the aim had been to elevate biomass concentrations and consequently raise volumetric productivities by utilising different biofilm immobilisation approaches. The studies consistently reported significant gains in product volumetric productivities, as compared to planktonic fermentations, however it is uncertain to what extent mass transfer effects were rate limiting. Increased biomass development inherently causes significant increases in biofilm thicknesses which, as a consequence of mass transfer limitations, would likely result in substrate depleted- and/or SA saturated zones within the aforementioned biofilms. Mass transfer limitations not only lead to inefficient use of biocatalysts but also result in process instabilities due to disintegration of biofilms [15]. This is likely one of the reasons Maharaj et. al. [9] reported difficulties in reaching and maintaining steady state at high dilution rates, due to frequent biofilm shedding events.

Internal mass transport limitations in biofilms are largely dependent on biofilm composition and properties such as porosity and cohesiveness [15]. Dense biofilms are characterised by slow diffusion rates whereas porous biofilms promote diffusion [18]. In addition, extracellular polymeric substances (EPS) in biofilms impede diffusion, a problematic property in pathogenic biofilms as it increases resistance to antimicrobial treatments [19]. Previous studies [20–22] have shown how both composition and properties of *A. succinogenes* biofilms vary depending on the hydrodynamic shear- and accumulated acid conditions. Low shear conditions would

result in porous structures and be favourable in terms of mass transfer but tend to be unstable and prone to shedding events [23–25]. On the other hand, dense biofilms formed in high shear conditions are known to be stable while limiting diffusion rates [23–25]. Central to the successful implementation of bulk microbial production of SA is the development of biofilms that are stable but do not limit potential productivities.

This work investigated internal mass transfer in biofilms of *A. succinogenes* by initially developing a theoretical transient internal mass transfer biofilm model, using intrinsic SA production kinetics estimated from resuspended batch biofilm fermentation experiments (i.e. to eliminate mass transfer limitations) in concert with known *A. succinogenes* biofilm properties [20–22]. The model was validated by accurate prediction of experimental transient batch biofilm behaviour. Subsequently, the model was extended to pseudo-steady state continuous operational conditions and used to assess how acid conditions, changes in biofilm density and composition, as well as biofilm thicknesses would affect glucose (Glc) availability and SA production effectiveness. Finally, a simplified method was proposed for the evaluation of pseudo-steady state Glc penetration thickness and active biofilm effectiveness; a tool for the design and optimisation of SA producing *A. succinogenes* biofilm-reactors.

2. Materials and Methods

2.1 Microorganism and fermentation media

Wild-type *Actinobacillus succinogenes* 130Z (DSM No. 22257; ATCC No. 55618) was acquired from the German Collections of Microorganisms and Cell Cultures (Braunschweig, Germany). Stock cultures (1.5 mL) were maintained at −40 °C in 66% v/v glycerol solutions. Inoculum was prepared by transferring a stock culture to 15 mL of sterilised tryptone soy broth at 30 g L^{-1} and incubating at 37 °C and 120 rpm for 16 to 24 h. Prior to inoculation, the

inoculum was analysed for purity by checking for consistent metabolite distribution using High-performance liquid chromatography (HPLC).

The fermentation medium was a replica of the medium developed by Bradfield & Nicol [12]. All chemicals were obtained from Merck KGaA (Darmstadt, Germany) unless otherwise stated. The fermentation medium consisted of three parts: the nutrient and salts solution, a phosphate buffer, and the Glc solution. The nutrient and salt solution was composed of: 10.0 g L^{-1} of clarified corn steep liquor (Sigma-Aldrich, St. Louis, USA), 6.0 g L^{-1} yeast extract, 0.5 g L^{-1} NaCl, 0.2 g L^{-1} $MgCl{\cdot}6H_2O$, 0.2 g L^{-1} $CaCl_2{\cdot}2H_2O$, and 10 mL L^{-1} antifoam SE-15 (Sigma-Aldrich, Germany). The phosphate buffer consisted of 3.2 g L^{-1} KH_2PO_4 and 1.6 g L^{-1} K_2HPO_4. The Glc concentration was maintained at 80 g L^{-1} except for one fermentation (batch run no: 3) wherein 125 g L^{-1} was used. CO_2 (Afrox, South Africa) was fed to the fermenters at 0.1 vvm.

2.2 Bioreactor

The same silicone tube bioreactor presented in the studies by Brink & Nicol [10,26] was used for fermentations in this study. The reactor consisted of a 3 mm diameter silicon tubing of approximately 5 m in length, with an active volume that ranged from 50 – 70 mL depending on the gas hold-up at the time. Gas hold-up was determined as the difference between the liquid volume at steady state and the total reactor volume. Temperature and pH were controlled at 37.0 ± 0.1 °C and 6.80 ± 0.01 respectively. A Liquiline CM442 (Endress+Hauser, Gerlingen, Germany) coupled to a Ceragel CPS71D glass electrode (Endress+Hauser, Gerlingen, Germany) measured both temperature and pH, and controlled pH by dosing of a 10 M NaOH solution by a peristaltic pump connected to an internal relay. Temperature was controlled by a feedback PID controller, custom developed in Labview. All gas vents and inlets were fitted

with 0.2 μm PTFE membrane filters (Midisart 2000, Sartorius, Göttingen, Germany) to ensure sterility.

2.3 Batch fermentations

All batch fermentations performed were preceded by a continuous fermentation period in which the biofilm was established. Continuous operation mode lasted for a period ranging from 36h to 66h. After the biofilm was developed and pseudo-steady state conditions were achieved, a switch was made to batch operation. A sample was taken at the onset of the batch fermentation to note initial conditions for a batch run. The product outflow and feed inlet pumps were switched off to initiate batch fermentation operation. For batch 1 to batch 3, the developed biofilm was intact on the inner walls of the silicone tube reactor during the entire batch fermentation to test for mass transfer restriction effects. To establish baseline conditions, i.e. "mass transfer free" conditions, two repeat runs (batch 4 and 5) were performed in which the developed biofilm was mechanically loosened from the inner silicon walls and mixed at high shear velocities until homogenous to simulate a free cell environment. External compression and simultaneous abrasion of the silicone tube reactor effectively detached the biofilm from the inner silicon walls. The recirculation velocity of the reactor volume was kept sufficiently high to prevent biofilm cell re-attachment on the surface throughout the course of the suspended batch fermentations. At the end of each batch fermentation, total biomass concentration was determined by sampling the entire volume of the reactor, taking care to remove all the attached biomass (batch 1 - 3). The sampled biomass was further treated to extract EPS (see EPS extraction section) and thus determine the fraction of the biofilm which consisted of cellular biomass. Table 1 gives a summary of pseudo-steady state conditions which preceded the onset of batch fermentations for all the runs.

Table 1: Summary of initial bulk concentrations of Glc ($C_{Glc,aq}$), SA ($C_{SA,aq}$), acetic acid ($C_{AA,aq}$), and formic acid ($C_{FA,aq}$) prior to initiation of batch fermentations.

	Total Biomass ($g.L^{-1}$)	Biofilm Cellular biomass ($g.L^{-1}$)	Total cellular biomass[1] ($g.L^{-1}$)	$C_{Glc,aq}$ ($g.L^{-1}$)	$C_{SA,aq}$ ($g.L^{-1}$)	$C_{AA,aq}$ ($g.L^{-1}$)	$C_{FA,aq}$ ($g.L^{-1}$)
Batch 1	12.01	6.01	7.83	68.24	6.95	3.70	1.78
Batch 2	7.32	7.01	7.64	66.23	9.63	4.80	2.54
Batch 3	10.51	4.83	7.30	113.59	9.35	4.12	1.61
Batch 4[2]	6.50	2.73	2.73	63.09	5.58	3.40	1.97
Batch 5[2]	5.93	2.65	2.65	58.46	6.14	4.27	2.89

[1]Includes cellular biomass from the biofilm and suspended cellular biomass
[2]Free cell fermentation

2.4 EPS extraction.

EPS was extracted from the sampled biofilm using the cation exchange resin (Dowex® Marathon® C sodium form, Sigma-Aldrich, Germany) method; it is reported to result in minimal cell lysis. For separation 10 mL of the harvested biomass sample was poured in a 50 mL Duran bottle with 10 g of cation exchange resin (CER) and a magnetic stirrer. The mixture was stirred at 600 rpm for 60 min at 4 ℃. After allowing for the decanting of the solid CER the liquid phase was carefully removed and centrifuged at 20000g for 30 min at temperature of 4 ℃. The cell precipitate was then dried in the oven at 70 ℃ until a constant measured mass remained. The difference between the total dry biomass weight and the total dry cell weight was determined as the EPS component of the biomass.

2.5 Analytical methods

Concentrations of Glc, ethanol, and organic acids – SA, acetic acid (AA), formic acid (FA), pyruvic acid (not reported) – in the fermenter broth were determined by High-Performance Liquid Chromatography (HPLC). An Agilent 1260 Infinity HPLC (Agilent Technologies, USA), equipped with an RI detector and a 300 mm × 7.8 mm Aminex HPX-87H ion exchange column (Bio-Rad Laboratories, USA) was used. Two mobile phases were used for two methods of analysis. The first method consisted of a 5 mM H_2SO_4 mobile phase solution fed at a flowrate of 0.6 mL min^{-1} and the second method used a 20 mM H_2SO_4 mobile phase at the same flowrate. The second method improved the accuracy of the Glc reading by separating the phosphate, Glc and pyruvic acid peaks.

2.6 Theory and model development.

This section presents the mathematical equations and assumptions used to model internal mass transport in the biofilm of *A. succinogenes*. A fixed film biofilm bioreactor system is considered in this study. Since continuous bioreactor operation at pseudo-steady state conditions preceded batch operation, both operation modes are considered in the model as the former is necessary to evaluate initial metabolite and substrate concentrations in the biofilm prior to the onset of batch fermentation.

2.6.1 A. succinogenes kinetic model description

Specific growth rate of *A. succinogenes* was modelled using product inhibition kinetics described by a Gompertz asymmetrical sigmoid function as reported, and validated against prominent studies on *A. succinogenes*, in the study by Brink and Nicol [10]. Lin et al. [4] reported a low Monod substrate saturation constant indicating that *A. succinogenes* specific

growth rate has a low dependence on the substrate concentration and therefore justifying the choice for solely using product inhibition kinetics.

$$\boldsymbol{\mu = 0.82\left(1 - \ e^{-6e^{-0.54C_{SA}}}\right)} \quad (1)$$

Equation 1 incorporates a maximum specific growth rate (μ_{max}) of 0.82 h^{-1} and SA concentration (C_{SA}) as the product inhibition variable. C_{SA} is a good proxy variable for inhibition as growth appears to be strongly influenced by the C_{SA}. As the major product, it is therefore reasonable that SA would be the major contributor to inhibition. The cell-based production rate of SA (r'_{SA}) was simulated by a combination of growth associated (ϕ) and maintenance associated (θ) production rates, as expressed in Equation 2 and 3, [4,10].

$$\boldsymbol{r'_{SA} = \phi\mu + \theta} \quad (2)$$

$$\boldsymbol{\theta = \frac{kC_{SA}}{K_P + C_{SA} + \frac{C_{SA}^2}{K_I}}} \quad (3)$$

Equation (3) shows that the maintenance associated production rate was not modelled as a constant value but as a decreasing function with increasing C_{SA} by using a modification of the Haldane inhibition model [27]. This is in line with numerous observations of decreasing r'_{SA} with increasing SA titres [9,12]. Figure 1 shows the ratio of production rates of AA to SA ($Y_{AA/SA}$) and those of FA to SA ($Y_{AA/SA}$) as function of bulk SA concentrations respectively, attained from prominent continuous fermentation studies of *A. succinogenes* [9,10,12,26,28].

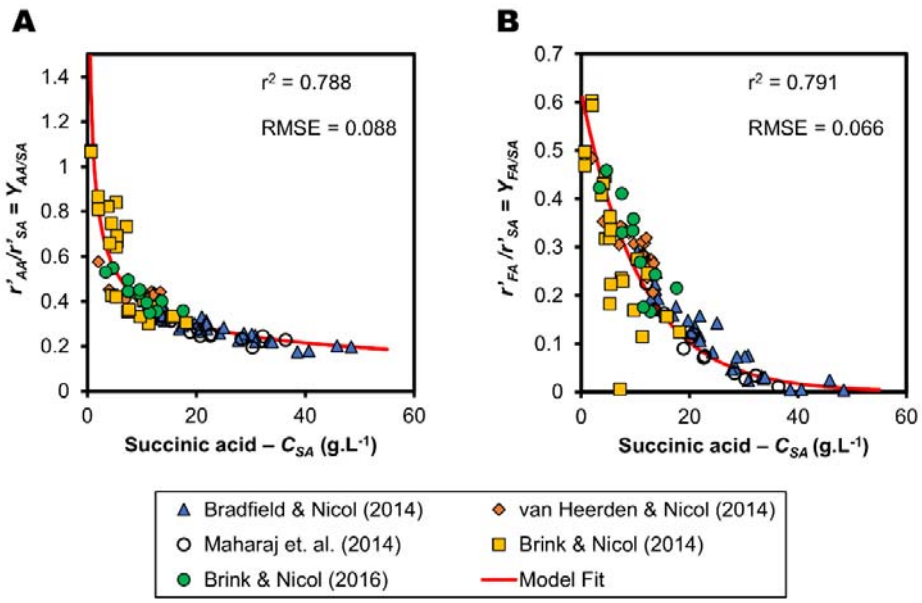

Figure 1: Pseudo-steady state production rate ratios of AA to succinic acid (A) and FA to succinic acid (B). Data was obtained from prominent continuous biofilm fermentation studies [9,10,12,26,28].

The mass ratio functions obtained were used to relate the SA production rate to the AA and FA production rates, as given in Equation 4 and 5 below.

$$r'_{AA} = Y_{\frac{AA}{SA}} r'_{SA} \tag{4}$$

$$r'_{FA} = Y_{\frac{FA}{SA}} r'_{SA} \tag{5}$$

The mass ratios are a function the C_{SA} given in Equation 6 and 7 (from Figure 1).

$$Y_{\frac{AA}{SA}} = 1.112 C_{SA}^{-0.445} \tag{6}$$

$$Y_{\frac{FA}{SA}} = 0.6214 e^{-0.09 C_{SA}} \tag{7}$$

The Glc consumption rates were determined using an electron balance given the production rates of the by-products (Equation 8). In this balance, the electrons donated by Glc must be captured by the by-products and as such a degree of reduction balance on a C-mol basis [29] is used to solve for the Glc consumption rate as shown. To account for minor by-products,

specifically pyruvic acid, these were expressed in terms of mass of FA using an equivalent electron base and incorporated in the production rate of FA in equation 8.

$$r'_{GLUC}\left(\frac{4}{30}\right) = r'_{SA}\left(\frac{3.5}{29.5}\right) + r'_{AA}\left(\frac{4}{30}\right) + r'_{FA}\left(\frac{2}{46}\right) \quad (8)$$

Combining equation 4 and 5 with equation 8, a simplified expression of Glc consumption rate can be expressed as:

$$r'_{Glc} = \left(0.89 + Y_{\frac{AA}{SA}} + 0.33Y_{\frac{FA}{SA}}\right) r'_{SA} \quad (9)$$

2.6.2 Pseudo-steady state concentration profiles under continuous biofilm operation

To calculate pseudo-steady state concentrations of the substrate and the metabolic products in the biofilm layer, the following assumptions were made.

- The geometry of the biofilm is assumed to be a uniformly thick planar slab with one side adjoined to an impermeable substratum surface and the other side exposed to the bulk liquid phase.
- Components of the biofilm, i.e. the cells and the EPS as well as the water in the porous section of the biofilm are homogenously distributed throughout the biofilm.
- External mass transfer limitations between the biofilm and the liquid interface are neglected.
- Only one-dimensional internal mass transport is present and obeys Fick's Law

Under pseudo-steady state conditions, there is no mass accumulation within the biofilm layer, and as such the rate of reaction equals the rate of diffusion at any point in the biofilm. Equation 10 gives the general mass balance used to solve for the concentration profiles.

$$\boldsymbol{D_{e-j}}\ \frac{\boldsymbol{d^2C_j}}{\boldsymbol{dz^2}} = \boldsymbol{r'_j C_{XB}} \tag{10}$$

With the following boundary conditions,

$$\begin{cases} for\ z\ =\ L^*, & C_j\ =\ C_{j,aq} \\ for\ z\ =\ 0 & \dfrac{dC_j}{dz} = 0 \end{cases}$$

The system of second order differential equations describing the concentrations of products and the substrate was solved numerically with an iterative procedure using a finite difference method. More details regarding the discretisation of the system are presented in the Supplementary Information.

Note: In the pseudo-steady model, L^* indicates the biofilm thickness that has access to Glucose and are therefore considered to be biologically active. Any biofilm beyond this thickness would be depleted of glucose and could therefore be assumed biologically inactive/dead, i.e. the real/active catalyst thickness cannot be greater than L^*.

2.6.3 Batch operation model description

The batch system consists of the bulk liquid phase and the biofilm phase. In the liquid phase suspended cells grow and convert the substrate to products and there is diffusion of metabolic products and the substrate to and from the biofilm phase, respectively. Equation 11 and 12 give a generic mass balance in the liquid phase.

$$\frac{\boldsymbol{dC_{j,aq}}}{\boldsymbol{dt}} = \boldsymbol{r'_j C_{X,aq}} + \boldsymbol{J_j} \tag{11}$$

$$\boldsymbol{J_j} = \boldsymbol{D_{e-j} A_p} \frac{\boldsymbol{dC_j}}{\boldsymbol{dz}}\Big|_{\boldsymbol{z=L}} \tag{12}$$

In the biofilm phase, the general mass balance is presented in Equation 13

$$\frac{dC_j}{dt}|_z = -D_{e-j}\frac{d^2C_j}{dz^2} + r'_j C_{XB} \quad (13)$$

The batch system of equations was simulated using numerical methods by discretising the system of equations. The detailed description of the discretised system used is given in the Supplementary Information.

2.6.4 Estimation of the effective diffusivity, De

The parameter $D_{e\text{-}j}$ represents the effective diffusion constant of compound *j* in the biofilm as related to the aqueous diffusion constant. Effective diffusivity constants were estimated for each metabolic product and the substrate using a mathematical model proposed by Hinson and Kocher [24] specifically developed for determining effective diffusivities in biofilms (equation 14 to 16). The model uses the biofilm volume fractions of the cells (ε_{cells}), EPS (ε_{EPS}), and water (ε_W) to estimate diffusivities ($\varepsilon_{cells} + \varepsilon_{EPS} + \varepsilon_W = 1$). It was assumed that wet biofilm consisted of 90% water on a volume basis.

$$\frac{D_{eo-j}}{D_{aq-j}} = \varepsilon_W\left[\frac{\varepsilon_{EPS}}{D_{pr}} + \varepsilon_W\right]^{-1} \quad (14)$$

$$\frac{D_{e-j}}{D_{aq-j}} = \left(\frac{D_{e-j}}{D_{eo-j}}\right)\left(\frac{D_{eo-j}}{D_{aq-j}}\right) \quad (15)$$

$$\frac{D_{e-j}}{D_{eo-j}} = \left[\frac{\frac{2}{D_{cr}} + \frac{D_{aq-j}}{D_{eo-j}} - 2\varepsilon_{cells}\left(\frac{1}{D_{cr}} - \frac{D_{aq-j}}{D_{eo-j}}\right)}{\frac{2}{D_{cr}} + \frac{D_{aq-j}}{D_{eo-j}} + \varepsilon_{cells}\left(\frac{1}{D_{cr}} - \frac{D_{aq-j}}{D_{eo-j}}\right)}\right] \quad (16)$$

3. Results and Discussions

3.1 Batch fermentations

Figure 2 presents batch profile results for C_{SA}, C_{Glc}, C_{AA}, and C_{FA} attained in the free cell batch fermentation experiments (batches 4 and 5). Initial batch conditions for these runs can be found in Table 1. Since biomass measurements were only taken at the end of each fermentation,

uncertainty exists in the initial biomass concentrations for all batch fermentations, however as all fermentations operated at C_{SA} greater than 10 $g.L^{-1}$ for more than 90% of the runs, it is assumed that negligible biomass growth took place due to severe product inhibition [10]. Repeatable results were obtained for all the metabolic products as well as the C_{Glc} profile, as seen in Figure 2. No lag phases were observed since batch fermentations were preceded by continuous fermentation operation for biofilm development. Prior to the inception of the batch operation of batches 4 and 5, however, biofilm cells were mechanically loosened from the inner silicon walls and mixed at high shear velocities until homogenous to emulate free cell batch fermentation. The concentration profiles in Figure 2 where used to estimate the intrinsic "mass transfer free" kinetic model parameters for Equations 2 to 3, the fitted parameters are presented in Table 2. As can be seen in Figure 2E, the kinetic model gave a good prediction of the C_{SA}, C_{Glc}, C_{AA}, and C_{FA} curves – estimated coefficient of determination (r^2) = 0.984 and root-mean-square error (RMSE) = 2.12 $g.L^{-1}$. The shaded area in Figure 2E shows the 99% prediction band. The prediction band is defined as the interval for a given independent variable within which future observations are expected to lie with a specific probability (in this case 99%), given historical observations and assuming a normal distribution of errors [30]. Prediction intervals are directly related to the standard deviations of the observations; the narrow prediction interval in Figure 2E (±5.611 $g.L^{-1}$) indicate a small standard deviation between the measured and predicted values and consequently a relatively low uncertainty in the model [30].

Table 2: Estimated intrinsic kinetic model parameters for equations 2 and 3

Parameters	Value	Units	Equation
ϕ	3.60	$g.g^{-1}$	2
k	3.00	$g.g^{-1}.h^{-1}$	3
K_P	13.15	$g.L^{-1}$	3
K_I	7.52	$g.L^{-1}$	3

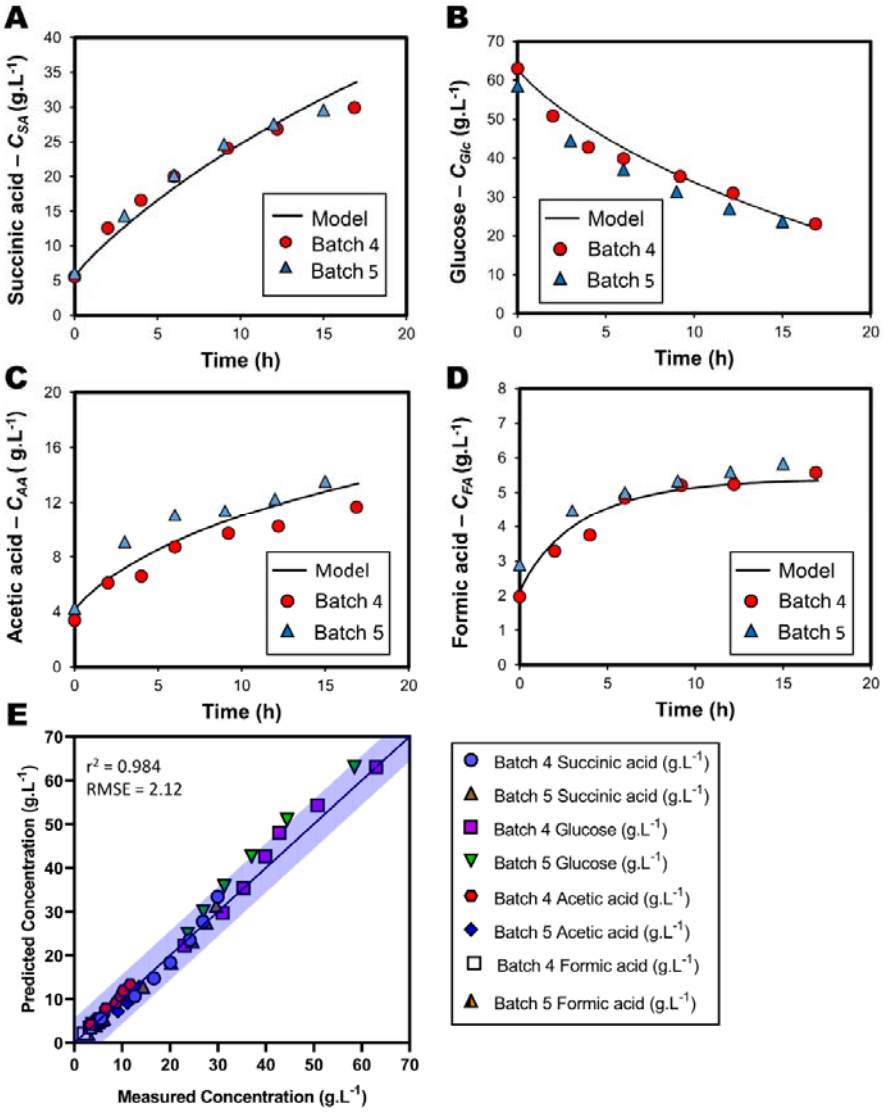

Figure 2: Resuspended biofilm "free cell" batch fermentation concentration profiles for (A) SA, (B) Glc, (C) AA, and (D) FA. The solid line shows the predicted concentrations according to the intrinsic kinetic model. (E) shows the parity plot of the predicted metabolite and substrate concentrations vs the measured concentrations. The shaded area in (E) shows the 99% prediction band for the model; i.e. future measurements have a 99% probability of falling within this band.

The batch mass transfer model presented in section 2.6.3 was used to simulate mass transfer effects in batches 1, 2, and 3. To this end, the final total dry biofilm biomass measurements (Table 1) were used to estimate the total biofilm thickness (L) and assuming that dry biomass constituted 10% of the wet biofilm weight, with a homogenous distribution of biofilm across

the entire inner silicon tube area with a fixed thickness. The initial concentrations within the biofilm were solved by using the pseudo-steady state model presented in section 2.6.2.

The results for the simulation are shown in Figure 3 as solid lines in the $C_{SA,aq}$, and $C_{Glc.aq}$ graphs for batches 1, 2, and 3. Similar trends were observed for $C_{AA,aq}$ and $C_{FA,aq}$ profiles (not reported). Figure 3 A – F further show both models with and without the inclusion of mass transfer effects – demonstrating the impact of mass transfer on the $C_{SA,aq}$ and $C_{Glc,aq}$. It can be seen that by accounting for internal mass transfer effects within the biofilm, good predictions were attained (in Figure 3) which closely followed the observed measured concentration profiles. Table 3 statistically compares the goodness of the model predictions (with and without internal mass transfer) by analysing the r^2 and the RMSE for model predictions of succinic acid and glucose against measured experimental data for biofilm batches 1 – 3. Accounting for internal mass transfer significantly improves the RMSE of the predicted metabolites, especially considering that biofilm effectiveness factors were as high as 75% to 97% for batches 1 – 3.

These results verified the presence of mass transfer effects in batches 1 – 3 and that the mass transfer effects were accurately predicted by the internal mass transfer batch model. In addition, the Hinson and Kocher [31] mathematical model accurately predicted the effective diffusivities of metabolic products and the substrate within the biofilm.

Table 3: Comparison of goodness of model prediction for glucose and succinic concentration

Experiment	Statistical goodness of fit	Succinic acid		Glucose	
		Mass transfer model	Intrinsic rate model (no mass transfer)	Mass transfer model	Intrinsic rate model (no mass transfer)
Batch 1	R^2	0.9836	0.9291	0.9765	0.9132
	RMSE	2.496	6.153	3.84	7.578
Batch 2	R^2	0.9691	0.9647	0.9837	0.9488
	RMSE	3.328	4.155	3.128	5.651
Batch 3	R^2	0.995	0.9501	0.9648	0.9603
	RMSE	1.666	6.161	6.651	8.443

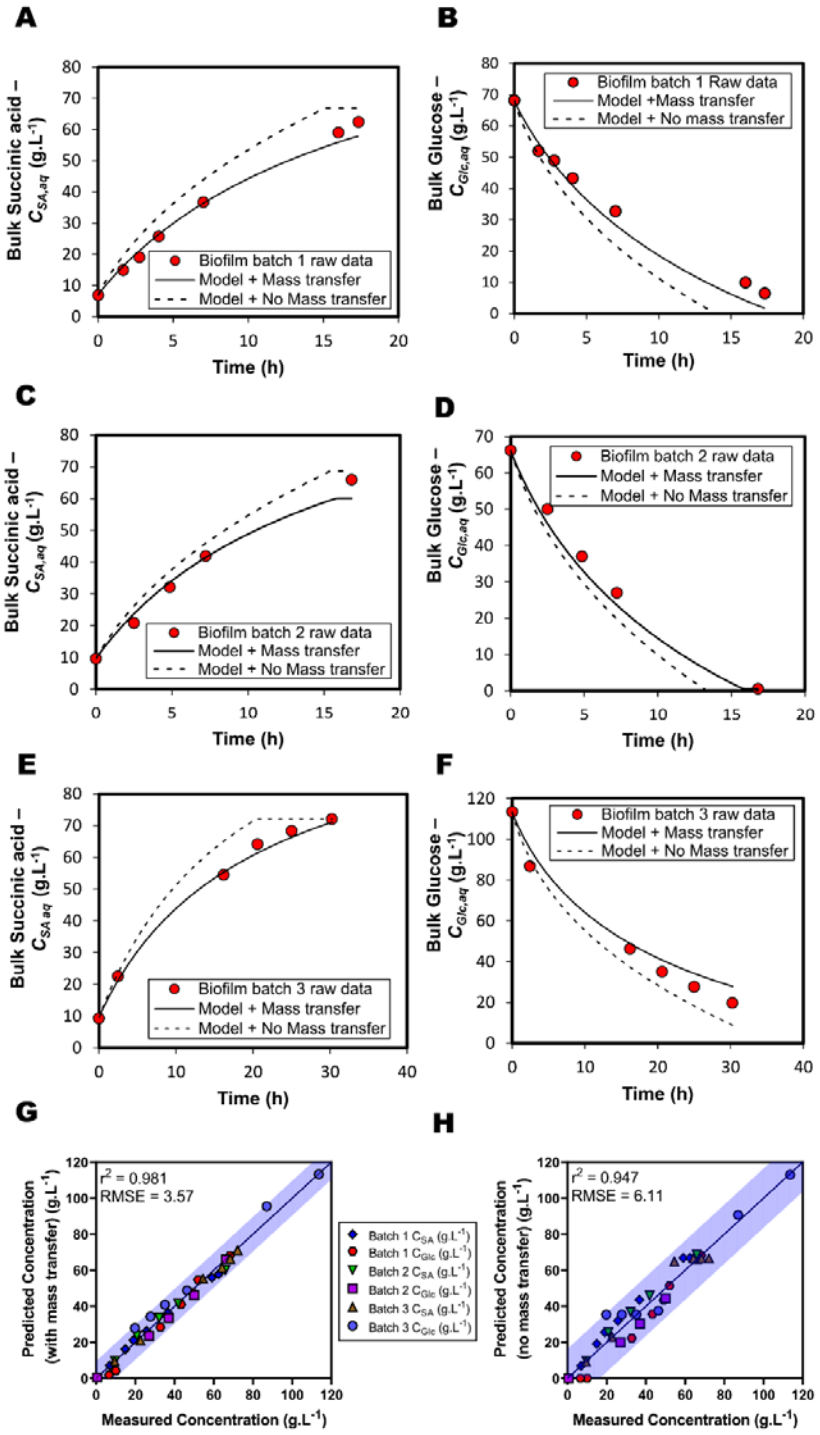

Figure 3: Biofilm batch bulk concentration profiles for SA (A, C, and E) and Glc (B, D and F) for batches 1 to 3. The dotted lines show the predicted concentration profiles according to the developed intrinsic kinetic model. The solid lines show the concentration profiles obtained when internal mass transfer in the biofilm is accounted for. G: Parity plot of the Model + Mass transfer vs experimental data. H: Parity plot of the Model + No Mass transfer vs experimental data. The shaded areas in G and H and show the 99% prediction bands; a significantly narrower prediction band is observed in G vs H (±9.58 g.L^{-1} vs ±16.39 g.L^{-1}) indicating a smaller standard deviation and consequently a significantly better fit.

It should be noted that SA reached maximum titres of between 62 g.L^{-1} and 72.1 g.L^{-1} for batch 1, 2, and 3 respectively, compared to maximum titres of 29.9 g L^{-1} and 29.6 g L^{-1} SA for free cell batch fermentations (Figure 2). Low total cellular biomass in free cell batch fermentations (2.73 gDCW.L^{-1} and 2.65 gDCW.L^{-1}) as compared to higher total cellular biomass in biofilm batch runs (7.83 gDCW.L^{-1}, 7.64 gDCW.L^{-1}, and 7.3 gDCW.L^{-1}) as well as the increased inhibitory effects with increased SA titres (see equations 1 and 3) caused distinct differences in observed maximum SA titres. Moreover, as can be seen in Figure 3, the simulated batch profiles for biofilm batch 1, 2, and 3 according to the intrinsic "mass transfer free" kinetic model predicted faster rates than experimentally observed. The simulated biofilm batch profiles, without consideration of mass transfer, reached the final titre conditions two hours earlier for batch 1 (Figure 3A), one hour earlier for batch 2 (Figure 3C) and nine hours earlier for batch 3 (Figure 3E), than was measured in the bulk of the reactor. These results clearly showed that mass transfer effects resulted in suppressed volumetric productivity rates.

3.2 Impact of internal mass transfer on production rates and biocatalyst effectiveness in batch biofilm fermentations

In Figure 4A, the intrinsic r'_{SA} according to the kinetic model (fitted from free cell fermentation results) is compared with the r'_{SA} of biofilm batches 1, 2, and 3, all as a function of SA titre. For batch 1 and 3 runs, the r'_{SA} was consistently lower than the intrinsic r'_{SA} throughout most of the fermentation period. Conversely, for batch 2 lower r'_{SA} were attained only until a SA titre of 30 g.L^{-1} was reached, after which the r'_{SA} was equal to the intrinsic r'_{SA} throughout. This suggested that batch 2 experienced mass transfer effects only in the beginning stages of the batch fermentation (first 5 hours), after which intrinsic kinetics were observed.

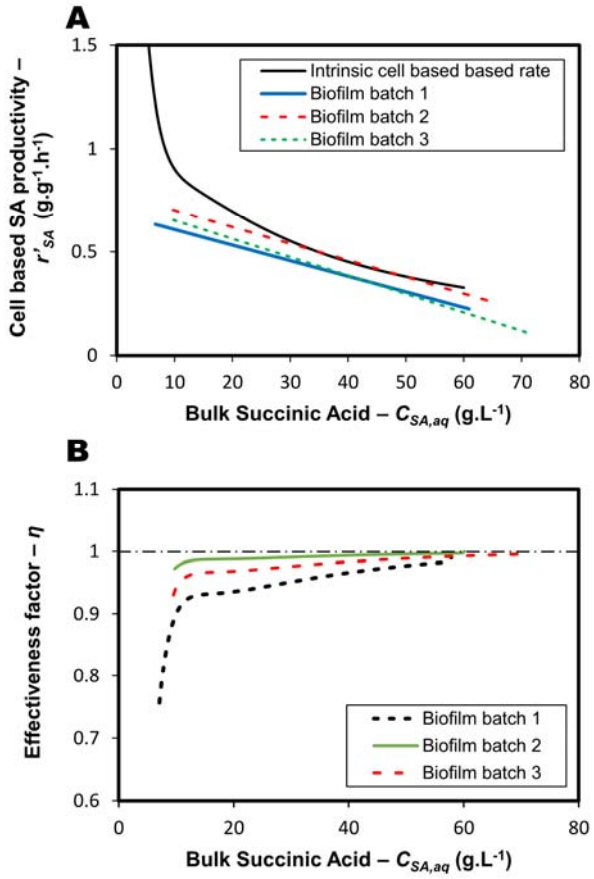

Figure 4: A: Comparison of cell-based SA productivity as function of SA titres in bulk phase for biofilm batches with the intrinsic rates. B: Biofilm effectiveness factor during batch operation as function of bulk SA titres.

Concentration profiles of Glc and metabolic products throughout the biofilm thickness were predicted for each time point in the batch simulations. Figure 5 shows C_{SA} and C_{Glc} profiles in the biofilm thickness at select time points, the dashed lines indicate the bulk concentrations in the reactor, i.e. at a biofilm thickness of 0 µm. Gradients of both C_{Glc} and C_{SA} within the biofilm are higher at the start of fermentation and consequently decrease with time for all batches. Metabolite gradients were steeper in batch 1 followed by batch 3, and significantly low gradients were observed in batch 2. It is reasonable that less mass transfer effects were observed in batch 2 as it attained the lowest estimated biofilm thickness (120 µm) as well as the lowest fraction of EPS in the biofilm (0.03). Moreover, mass transfer effects were dominant in batch 1 where the maximum estimated biofilm thickness of 205 µm was observed. Decreasing

gradients within the biofilm with time make sense as increasing C_{SA} decreases cell-based rates due to product inhibition, thus the difference between diffusion rates and reaction rates is reduced.

An effectiveness factor (η) was computed as the ratio of the average r'_{SA} in the biofilm to the r'_{SA} at bulk SA conditions, Equation 17. The η parameter quantifies the mass transfer effects present in the biofilm; the closer to unity the less the mass transfer limitations experienced by the biofilm, and *vice versa*. Note: The η values indicate the effectiveness of the L^* therefore ignoring any additional biologically inactive biofilm. In the case of the batch results $L^* = L$ for all measured conditions.

$$\boldsymbol{\eta} = \frac{\boldsymbol{r'_{SA,avg}}}{\boldsymbol{r'_{SA,aq}}} \tag{17}$$

The C_{SA} profiles, shown in Figure 5, were used to calculate the effectiveness factors of the biofilm throughout the batch fermentations and are shown Figure 4B. The effectiveness factor of the biofilm in batch 1 ranged from 75% at the beginning of the batch to 99% at the end of fermentation, from 97% to 100% for batch 2, whereas for batch 3 the biofilm had an effectiveness factor which ranged from 92% to 100%. Mass transfer effects where nearly negligible in batch 2. In batch 1, however, the biofilm began with a low effectiveness factor of 75% which was most likely caused by low initial SA titres of 6.95 $g.L^{-1}$ whereas for both batch 2 & 3, SA titres started at 9.63 and 9.35 $g.L^{-1}$, respectively. The subsequent rapid increase in the effectiveness factor at the early stages of batch 1 is due to the quick change in acid conditions which reduced reaction rates as a result of product inhibition.

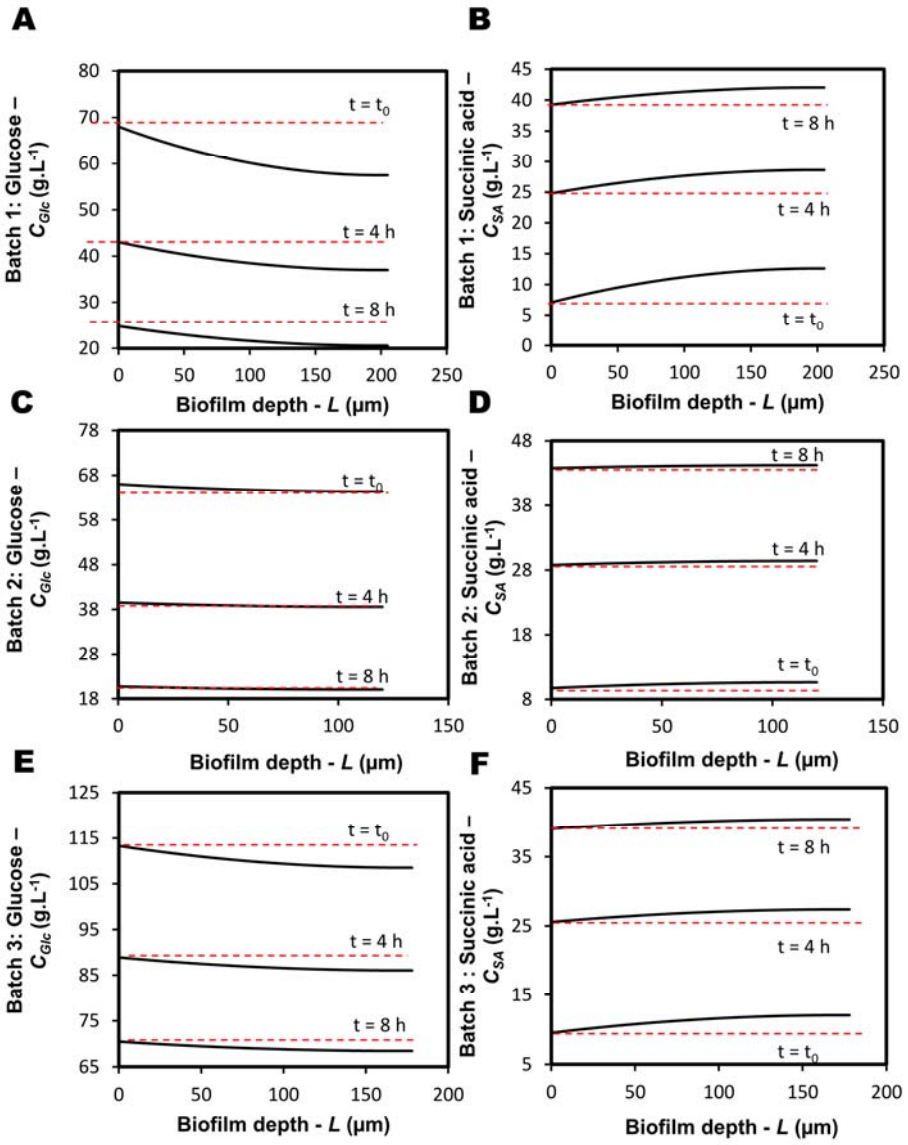

Figure 5: Concentration profiles of Glc (A, C and E) and SA (B, D and F) in the biofilm at selected times.

3.3 Expanded analysis of the model at pseudo-steady state conditions

In this section the pseudo-steady state model (section 2.6.2) was used to gain insight into the influence of the biofilm properties and reaction conditions on the overall effectiveness of the biofilm during continuous pseudo-steady state fermentations. The complex nature of the model required a method to combine the interactions of the various parameters in a mechanistically interpretable way. A data set of pseudo-steady state biofilm results was compiled by combining results for pseudo-steady state fermentation studies by Maharaj et al. [9], Brink & Nicol

[10,26], Mokwatlo et al. [21] (**Error! Reference source not found.**), and a generated set of realistic pseudo-steady state biofilm conditions (Supporting Information – Table S - 1). The data were chosen specifically because it included a significant variation in the shear conditions, biofilm biomass composition, total biomass concentrations (which affects thicknesses), and pseudo-steady state SA and Glc titres.

The conditions for each pseudo-steady state was modelled using the pseudo-steady state model from section 2.6.2. The relationships between individual system variables ($C_{SA,aq}$, $C_{Glc,aq}$, $C_{XB,}$ $\varepsilon_{W,}$ and ε_{EPS}) and the overall biofilm effectiveness (η), as predicted by the pseudo-steady state model (section 2.6.2), are shown in the Supporting Information (Figure S – 1). The Pearson correlation coefficient heat map in Figure S – 1 show that poor correlation was observed between η and the system variables.

Traditionally, catalyst effectiveness is related by a Thiele modulus – a dimensionless factor reflecting the ratio of reaction rate to the rate of diffusion in the catalyst [32,33]. Thiele moduli are derived by expressing the pseudo-steady state component balance in a dimensionless format [32,33]. To obtain the equivalent of the Thiele modulus for the *A. succinogenes* biofilm (α^2), SA was used as a proxy variable in the pseudo-steady state internal mass transfer balance given in Equation 10 due to its impact on *A. succinogenes* kinetics. In addition, Equation 10 was further simplified by neglecting growth associated SA production; the range of SA titres of industrial interest are $\gg$ 10 g.L^{-1} and growth is negligible above 10 g L^{-1} [10]. The pseudo-steady state component balance in Equation 10 was therefore simplified to dimensionless equation 18

$$\frac{dC_{SA}^*}{dZ^2} = \frac{\alpha^2 C_{SA}^*}{1+\beta C_{SA}^* + \gamma\beta C_{SA}^{*2}} \quad (18)$$

Where the non-dimensional SA titre – $C_{SA}^*$is defined by $\frac{C_{SA}}{C_{SA_{aq}}}$ and the non-dimensional active biofilm thickness Z is z/L^*. Non dimensional parameters α^2, β, and γ are given by $\alpha^2 = \frac{kL^{*2}C_{XB}}{D_{e-SA}K_P}, \beta = \frac{C_{SA_{aq}}}{K_P}$, and $\gamma = \frac{C_{SA_{aq}}}{K_I}$.

It is interesting to note the similarity between the dimensionless parameter α^2 and the traditional Thiele modulus for a first order reaction system. It can be concluded that at sufficiently low concentrations of SA the system will behave as a first order system. As SA increases the system will experience significant product inhibition as quantified by the dimensionless inhibition parameters β and γ and therefore deviating from first-order behaviour. To account for this inhibition on the system, a new dimensionless parameter (m) was defined (equation 19)

$$m = \sqrt{\frac{\alpha^2}{1+\beta+\gamma\beta}} \quad (19)$$

Equation 19 requires knowledge of the dimensionless parameter α^2 and consequently L^* preferably without the need to solve the overall mass transfer model. Stewart [15] defined a pseudo-steady state equation (equation 20) in which biofilm penetration can be calculated as the thickness at which the rate of diffusion of Glc into the biofilm equal the rate of consumption of the Glc within the biofilm, therefore resulting in full Glc depletion.

$$L^* = \begin{cases} \sqrt{\frac{2D_{e-Glc}C_{Glc,aq}}{r'_{Glc,avg}C_{XB}}}; \sqrt{\frac{2D_{e-Gluc}C_{Glc,aq}}{r'_{Glc,avg}C_{XB}}} < L \\ L; \sqrt{\frac{2D_{e-Glc}C_{Glc,aq}}{r'_{Glc,avg}C_{XB}}} \geq L \end{cases} \quad (20)$$

To solve equation 18 the $D_{e\text{-}Gluc}$ values were calculated using equation 14 to 16, $r'_{Glc,avg}$ values were calculated using equations 2 – 9, assuming an average C_{SA} represented by the logarithmic mean concentration difference between the bulk SA concentration and SA concentrations within the depths of the biofilm, i.e. at full Glc conversion. Chilton and Colburn [34] reported

that the mass transfer driving force can be estimated by the logarithmic mean concentration difference, analogous to heat transfer in heat exchangers. C_{XB} values were estimated by assuming the dry biofilm constituted 10% of the biofilm volume and an active biomass fraction of 0.35. The parity plot of the predicted L^* (Equation 20) and the L^* as obtained from the mass transfer model is shown in Figure 6A. It is clear from the correlation parameters (r^2 = 0.993, RMSE = 14.37 μm) and the narrow 99% prediction band (± 38.107 μm), a very good prediction for L^* was obtained from Equation 20.

The comparison of the parameter m (Equation 19) and η (Equation 17) for the pseudo-steady state data set (Table S – 1 and Table S – 2) is shown in Figure 6B. It was found that the m vs η data fit a segmental linear regression, i.e. two consecutive linear regressions described by equation 21. The regression parameters for the fit are shown in Table 4 and show that a very good fit was obtained with r^2 = 0.970 and RMSE = 0.0222. Considering the significant variability between the individual system parameters and η as shown in the Supporting Information (Figure S - 1), the quality of the linear regression was highly significant.

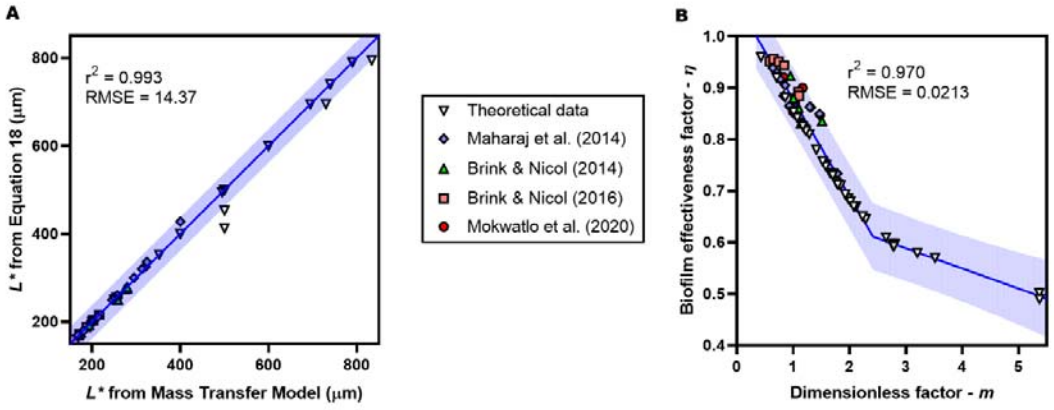

Figure 6: A: Parity plot of the L^* calculated using equation 20 vs L^* calculated using the internal mass transfer model for the pseudo-steady state data set. B: Effectiveness factor (η) as a function of dimensionless factor m showing a segmental linear regression for the pseudo-steady state data set. The shaded areas in in both A and B show the 99% prediction bands.

$$\eta = \begin{cases} a_1 m + c_1; 0.4 < m \leq m_o \\ a_2(m - m_0) + \eta(m_o)\,; m > m_o \end{cases} \quad (21)$$

Table 4: Optimised model parameters and fitting parameters for equation 19

Parameter	Value
a_1	-0.188
c_1	1.07
m_o	2.42
a_2	-0.0391
Degrees of Freedom	63
r^2	0.970
RMSE	0.0222

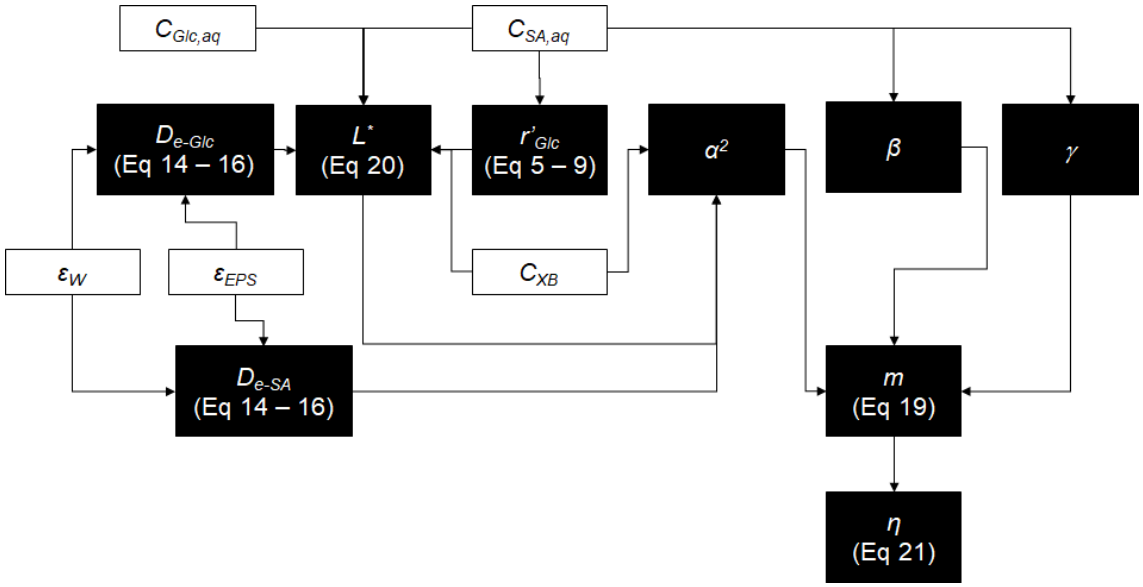

Figure 7: The proposed simplified algorithm for quantifying the mass transfer effects in a pseudo-steady state biofilm of *A. succinogenes*. The clear blocks represent inputs to the system and the shaded blocks show the calculated variables.

Following the derived relationships presented in equations 20 and 21, a simplified algorithm – shown diagrammatically in Figure 7 – is proposed for determining the impact of internal mass transfer on pseudo-steady state *A. succinogenes* biofilms. The inputs to the algorithm are $C_{SA,aq}$, $C_{Glc,aq}$, ε_W, ε_{EPS}, and C_{XB} (shown in the clear blocks). The shaded blocks indicate the calculated variables and the arrows show the interactions between different inputs and calculated variables. The most important outputs from the system are L^* and η which give a measure of the mass transfer effects on the biofilm system.

The power of equations 20 and 21 extend beyond the calculation of η and L^* values without the requirement to solve the complete mass transfer model. These equations provide insight into the interactions between different system variables resulting in L^* and η values and consequently provides potential understanding required for optimisation in terms of biofilm reactor design and/or operation.

To illustrate, selected data from Table S – 1 were chosen and analysed to assess the impact of the operational conditions on mass transfer in the biofilm. Within a biofilm system, the biofilm properties are a strong function of the history of the biofilm. Mokwatlo et al. [20,21] showed that metabolite accumulation, specifically C_{SA}, and external shear are major factors in the development of *A. succinogenes* biofilms. The data for Maharaj et al. [9] were obtained in a packed bed system under very low shear conditions (0.04 $m.s^{-1}$) and dilution rates between 0.054 and 0.72 h^{-1}, corresponding to SA titres between 32.5 $g.L^{-1}$ and 11 $g.L^{-1}$. The data for Brink & Nicol (2014) [10] were obtained at intermediate shear conditions (0.09 $m.s^{-1}$) and for dilutions rates between 0.51 and 1.0 h^{-1} (C_{SA} between 18.2 $g.L^{-1}$ and 12.3 $g.L^{-1}$), while Brink & Nicol (2016) [26] were obtained at intermediately high shear conditions (0.36 $m.s^{-1}$) at dilution rates of between 0.44 and 1.4 h^{-1} (C_{SA} between 17.6 $g.L^{-1}$ and 10.9 $g.L^{-1}$). Data for Mokwatlo et al. [21] were obtained at intermediately high and high shear conditions (0.36 and 0.64 $m.s^{-1}$) and at a dilution rate of 0.9 h^{-1} (C_{SA} at 11.6 and 14.9 $g.L^{-1}$, respectively). In each of these cases the two extreme dilution rates were selected therefore providing the extreme cases in terms of C_{SA} for each shear condition, except for Mokwatlo et al. [21] as the lowest dilution was at a titre below 10 g L^{-1}. Table 5 shows the selected conditions as well as the calculated values for applicable variables.

The results summarised in Table 5 show that for the lowest shear conditions (Maharaj et al. [9]) the high SA titre conditions translated to a significantly higher L^* than the low SA titre

conditions (295 μm vs 246 μm).` This can be attributed to a reduced ratio of Glc consumption rate to Glc diffusion rate in the high SA titre biofilm. The active biofilm thickness only covered between 51% and 42% of the overall thickness of the biofilm in the high and low SA titre systems. This implies that significant sections of the biofilm were Glc depleted.

The intermediate shear conditions (Brink & Nicol (2014) [10]) showed a significantly lower L^* for the high as compared to the low SA titre (258 μm vs 279 μm), the opposite effect seen for Maharaj et al. [9]. This observation was likely a result of the much lower SA titres than that observed by Maharaj et al. [9], resulting in a much greater Glc consumption rate in the biofilm and a concomitantly lower L^*. In this case the active layer of the biofilm was approximately equal for both dilution rates (83-86%), indicating a much healthier and more stable biofilm.

Table 5: Supplementary analysis of select pseudo-steady state results from the results reported in **Error! Reference source not found.** [9,10,21,26]

Shear velocity ($m\ s^{-1}$)	Dilution rate (h^{-1})	C_{SA} ($g.L^{-1}$)	L^* (Eq 20) (μm)	L^*/L (μm/μm)	η (Eq 19)	q_{SA} ($g.L^{-1}.h^{-1}$)	Source
0.04	0.054	32.5	295	0.51	0.91	1.76	[9]
	0.72	11.3	246	0.42	0.79	8.14	
0.09	0.51	18.2	258	0.83	0.88	9.28	[10]
	1.0	12.3	279	0.86	0.79	12.3	
0.36	0.44	17.6	159	1.00	0.96	7.74	[26]
	1.4	10.9	159	1.00	0.95	15.3	
0.64	0.9	14.85	196	1.00	0.91	13.4	[21]

At the relatively high shear conditions (Brink & Nicol (2016) [26], 0.36 $m.s^{-1}$) the biofilm L^* was at its lowest value, while full Glc penetration was observed for both SA titre conditions. Further analysis of the full set of results reported by Brink & Nicol (2016) [26] (**Error!**

Reference source not found.) showed complete glucose penetration for all dilution rates (results not shown). The high shear run by Mokwatlo et al. [21] did not result in the lowest L^* observed, but full Glc penetration was observed indicating a much-improved glucose transport with higher shear conditions.

To fully interpret the L^*-results requires analysis of equation 20. Equation 20 shows that L^* is dominated by the ratio of the diffusion rate of Glc through the biofilm to the consumption rate of Glc within the biofilm. This means that the greater the diffusion rate into the biofilm, the greater the L^*, however this would in turn lead to greater biomass growth rates and therefore a greater C_{XB} and $\overline{r'_{Glc}}$. The interplay between biomass growth and Glc diffusion would eventually lead to Glc depletion in the depths of the biofilm resulting in biofilm shedding events due to loss of biofilm structural integrity. Therefore, merely increasing the amount of biomass in the reactor, the usual objective in biofilm reactors, does not necessarily translate into the optimal bioreactor design and operation. For stable long-term operation it is imperative that L^* be maximised within the total biofilm.

To elucidate the complex nature of η requires in-depth analysis of equation 21 showing a direct negative proportionality between η and m; as m increases the mass transfer effects increase linearly (η decrease linearly). The m parameter has a positive dependence on α^2, while being inhibited by increasing C_{SAaq}. The α^2 parameter is in turn directly proportional to the L^* and C_{XB}, and inversely proportional to the SA diffusivity. From this it can be observed that the greater the active biofilm length and/or biomass concentration the greater the mass transfer impact, while an increased SA titre and -diffusivity reduces the mass transfer impact.

Considering the η values reported in Table 5, it is interesting to note that for the lowest shear conditions (Maharaj et al. [9]) a significantly improved η value at low dilution than the high

dilution conditions (0.91 vs 0.79) were observed. This indicates that the elevated SA titre (low dilution) countered the significantly larger L^* which consequently resulted in a much larger η value. For the intermediate shear conditions (Brink & Nicol (2014) [10]), the η values followed the same trend as that observed for Maharaj et al. [9], with a significantly greater biofilm effectiveness observed at higher SA titres as compared to the lower values. In this case the lower L^* also contributed to lower mass transfer effects, resulting in similar η. In the high shear biofilm experiments (Brink & Nicol (2016) [26] and Mokwatlo et al. [21]) much greater η values were observed for both SA titres (0.91-0.96), a consequence of the reduced L^*. This meant that comparable SA titres were measured to that in Brink & Nicol (2014) [10] even though much thinner biofilms with correspondingly lower biomass were observed under these elevated shear conditions.

The most striking impact of the high shear conditions can be seen when comparing the volumetric SA production rates (q_{SA}) at similar SA titres for the low- [9] and high shear [26] conditions. In these studies, SA titres of 11.3 $g.L^{-1}$ and 10.9 $g.L^{-1}$, and q_{SA} values of 8.14 $g.L^{-1}.h^{-1}$ and 15.3 $g.L^{-1}.h^{-1}$ were measured, respectively. This translates to an 88% increase in q_{SA} when comparing the high shear biofilm [26] to the lowest shear [9], even though the biofilm depths – and consequently biocatalyst present – were 36% lower. A very clear illustration of the effect of η on the production characteristics.

Overall, these results can be interpreted as follows: Since substrate gradients within biofilms grown at low SA titres are expected to be steep due to high reaction rates and excessive growth, biofilm starvation zones would likely result. As the biofilm matures the SA titres increase and the system tends to pseudo-steady state and frequent biofilm shedding events due to biofilm starvation at the base. High shear operation in these biofilm systems would prevent shedding events due to high eroding forces encountered therein which results in thinner and more stable

biofilms [35]. Mokwatlo et al [20] reported increased EPS production in dense biofilms developed at high shearing conditions acting as a mechanism for strengthening the biofilm. Additionally, the increased diffusional resistance due to higher EPS content would be countered by the thinner biofilm and consequently the negative effect on the biofilm effectiveness is negated.

It would be tempting to consider developing biofilm under high SA titre conditions to benefit from the high biofilm effectiveness earlier. However, Mokwatlo et al. [20] showed that biofilms grown in consistently high SA titre conditions (i.e. batch followed by low dilution rates) were intrinsically limited in terms of thickness and viability due to severe inhibitory effect of SA on *A. succinogenes*. This resulted in highly unstable biofilms even under low shear conditions. In the same paper it was mentioned that high acid titres completely inhibited biofilm formation at high shear conditions. This means that developing biofilms under high SA titre conditions is unfeasible for any shear conditions.

Considering that bulk SA fermentation production in industry will preferably occur at high SA titres for decreased downstream processing costs [36], mass transfer effects would inherently be significantly reduced. This means that the development of thin and dense biofilms grown under initially low SA titres and high shear conditions will grant more stability to the process while simultaneously increasing the biofilm effectiveness.**Conclusions**

The results attained in this study suggest that internal mass transfer has a significant impact on *A. succinogenes* biofilm fermentations. An intrinsic kinetic rate model – developed from a "mass transfer free" cell fermentation – was coupled to a reaction diffusion model to adequately model internal mass transfer restrictions in biofilm fermentations of *A. succinogenes.* The reaction diffusion model showed most pronounced internal mass transfer restrictions in the early stages of biofilm batch fermentations. These effects became less prominent due to

inhibition caused by elevated acid titres at later stages of batch fermentations. Biofilm biocatalyst effectiveness factor as low as 75% were observed at the start of batch fermentations. To quantify the effects of the complicated interactions on the active biofilm thickness and biofilm effectiveness a simplified algorithm is proposed; useful for design and optimisation purposes. Further analysis of the interactions of process variables showed that thinner biofilms developed at elevated shear conditions, when compared to thicker biofilms developed at low shear conditions, exhibited improved substrate penetration throughout the biofilm as well as higher biofilm effectiveness due to diminished mass transfer effects. This implies that exclusive focus on augmenting biomass concentrations within *A. succinogenes* biofilm reactors could be rendered redundant due to mass transfer effects.

Through utilisation of the proposed algorithm and internal mass transfer model the present study facilitates scaling of continuous SA production at high production rates in biofilm systems using *A. succinogenes*. To this end it is recommended that future study focus on the design and optimisation of bioreactor systems by quantifying (using the proposed algorithm and model) and manipulating (using SA titres and shear condition) the mass transfer effects within the *A. succinogenes* biofilm system.

Nomenclature

a_1	Slope of linear segment for $0.4 < m \leq m_o$ in equation 21	
a_2	Slope of linear segment for $m > m_o$ in equation 21	
AA	Acetic acid	
A_p	Surface area of biofilm in contact with bulk liquid phase	(m^2)
EPS	Extracellular polymeric substances	
FA	Formic acid	
c_1	Intercept of linear segment for $0.4 < m \leq m_o$ in equation 21	
C_j	Concentration of j	($g.L^{-1}$)
$C_{j,aq}$	Concentration of j in the bulk liquid phase	($g.L^{-1}$)
C_{SA}^*	Dimensionless SA concentration	
C_{XB}	Concentration of active biomass in the biofilm	($g.L^{-1}$)
D_{aq-j}	Diffusion constant of j in water	($m^2.s^{-1}$)
D_{cr}	Diffusivity of j in the cells relative to water	
D_{e-j}	Effective diffusion constant of j in the biofilm	($m^2.s^{-1}$)

D_{eo-j}	Effective diffusion constant of j in "cell free" EPS/water matrix	($m^2.s^{-1}$)
D_{pr}	Diffusivity of j in EPS relative to water	
Glc	Glucose	
J_j	Flux of j through the biofilm	($g.L^{-1}.h^{-1}$)
k	Maximum maintenance associated production rate	($g.g^{-1}.h^{-1}$)
K_P	Monod constant in the maintenance associated production rate	($g.L^{-1}$)
K_I	Inhibition constant in the maintenance associated production rate	($g.L^{-1}$)
L	Total biofilm thickness	(μm)
L^*	Biologically active biofilm thickness	(μm)
m_0	Point of interception on the m-axis of the line segments in equation 21	
m	Dimensionless parameter combining α^2, β, and γ	
qj	Volumetric production rate of j	($g.L^{-1}.h^{-1}$)
r'_j	Cell-based production rate of j	($g.g^{-1}.h^{-1}$)
$r'_{j,aq}$	Cell-based production rate of j in the bulk liquid phase	($g.g^{-1}.h^{-1}$)
$r'_{j,avg}$	Average cell-based production rate of j in the biofilm	($g.g^{-1}.h^{-1}$)

r^2	Coefficient of determination	
RMSE	Root-mean-square error	(Same dimensions as error)
SA	Succinic acid	
X	Active biomass	
$Y_{AA/SA}$	Ratio of production rates of AA to SA	($g.g^{-1}$)
$Y_{FA/SA}$	Ratio of production rates of FA to SA	($g.g^{-1}$)
z	Spatial perpendicular to the biofilm support structure	(m)
Z	Dimensionless active biofilm thickness	
α^2	Dimensionless Thiele modulus equivalent	
β	Dimensionless Monod constant K_P	
γ	Dimensionless inhibition constant K_I	
ε_{cells}	Volume fraction of cells in biofilm	
ε_{EPS}	Volume fraction of EPS in biofilm	
ε_W	Volume fraction of water in biofilm	
η	Biofilm effectiveness factor	
θ	Maintenance associated production rate	($g.g^{-1}.h^{-1}$)

μ	Specific growth rate of organism	(h^{-1})
μ_{max}	Maximum specific growth rate of organism	(h^{-1})
ϕ	Growth associated production rate coefficient	($g.g^{-1}$)

5. Acknowledgements

The financial assistance of the Sugar Milling Research Institute via the Step-Bio program is hereby gratefully acknowledged. The financial assistance of the National Research Foundation (NRF) towards this research is hereby acknowledged. Opinions expressed, and conclusions arrived at, are those of the author and are not necessarily to be attributed to the NRF.

6. References

[1] M. Ferone, F. Raganati, A. Ercole, G. Olivieri, P. Salatino, A. Marzocchella, Continuous succinic acid fermentation by Actinobacillus succinogenes in a packed-bed biofilm reactor, Biotechnol. Biofuels. 11 (2018) 1–11. https://doi.org/10.1186/s13068-018-1143-7.

[2] S. González-García, L. Argiz, P. Míguez, B. Gullón, Exploring the production of bio-succinic acid from apple pomace using an environmental approach, Chem. Eng. J. 350 (2018) 982–991. https://doi.org/10.1016/j.cej.2018.06.052.

[3] N. Shen, H. Zhang, Y. Qin, Q. Wang, J. Zhu, Y. Li, M.G. Jiang, R. Huang, Efficient production of succinic acid from duckweed (Landoltia punctata) hydrolysate by Actinobacillus succinogenes GXAS137, Bioresour. Technol. 250 (2018) 35–42.

https://doi.org/10.1016/j.biortech.2017.09.208.

[4] S.K.C. Lin, C. Du, A. Koutinas, R. Wang, C. Webb, Substrate and product inhibition kinetics in succinic acid production by Actinobacillus succinogenes, Biochem. Eng. J. 41 (2008) 128–135. https://doi.org/10.1016/j.bej.2008.03.013.

[5] P.C. Lee, S.Y. Lee, S.H. Hong, H.N. Chang, Isolation and characterization of a new succinic acid-producing bacterium, Mannheimia *succiniciproducens* MBEL55E, from bovine rumen., Appl. Microbiol. Biotechnol. 58 (2002) 663–8. https://doi.org/10.1007/s00253-002-0935-6.

[6] N. Samuelov, R. Datta, M. Jain, J. Zeikus, Samuelov, Datta, Jain, Zeikus, Whey fermentation by anaerobiospirillum succiniciproducens for production of a succinate-based animal feed additive, Appl. Environ. Microbiol. 65 (1999) 2260–3.

[7] E. Scholten, T. Renz, J. Thomas, Continuous cultivation approach for fermentative succinic acid production from crude glycerol by *Basfia succiniciproducens* DD1., Biotechnol. Lett. 31 (2009) 1947–51. https://doi.org/10.1007/s10529-009-0104-4.

[8] J.J. Beauprez, M. De Mey, W.K. Soetaert, Microbial succinic acid production: Natural versus metabolic engineered producers, Process Biochem. 45 (2010) 1103–1114. https://doi.org/10.1016/j.procbio.2010.03.035.

[9] K. Maharaj, M.F.A. Bradfield, W. Nicol, Succinic acid-producing biofilms of Actinobacillus succinogenes: Reproducibility, stability and productivity, Appl. Microbiol. Biotechnol. 98 (2014) 7379–7386. https://doi.org/10.1007/s00253-014-

5779-3.

[10] H.G. Brink, W. Nicol, Succinic acid production with Actinobacillus succinogenes: rate and yield analysis of chemostat and biofilm cultures, Microb. Cell Fact. 13 (2014) 111. https://doi.org/10.1186/s12934-014-0111-6.

[11] M.F.A. Bradfield, A. Mohagheghi, D. Salvachúa, H. Smith, B.A. Black, N. Dowe, G.T. Beckham, W. Nicol, Continuous succinic acid production by Actinobacillus succinogenes on xylose-enriched hydrolysate, Biotechnol. Biofuels. 8 (2015) 181. https://doi.org/10.1186/s13068-015-0363-3.

[12] M.F.A. Bradfield, W. Nicol, Continuous succinic acid production by Actinobacillus succinogenes in a biofilm reactor: Steady-state metabolic flux variation, Biochem. Eng. J. 85 (2014) 1–7. https://doi.org/10.1016/j.bej.2014.01.009.

[13] H. Song, S.Y. Lee, Production of succinic acid by bacterial fermentation, Enzyme Microb. Technol. 39 (2006) 352–361. https://doi.org/10.1016/j.enzmictec.2005.11.043.

[14] M. Ferone, F. Raganati, G. Olivieri, A. Marzocchella, Bioreactors for succinic acid production processes, Crit. Rev. Biotechnol. 39 (2019) 571–586. https://doi.org/10.1080/07388551.2019.1592105.

[15] P.S. Stewart, Diffusion in Biofilms, J. Bacteriol. 185 (2003) 1485–1491. https://doi.org/10.1128/JB.185.5.1485-1491.2003.

[16] Q. Yan, P. Zheng, J.J. Dong, Z.H. Sun, A fibrous bed bioreactor to improve the productivity of succinic acid by Actinobacillus succinogenes, J. Chem. Technol.

Biotechnol. 89 (2014) 1760–1766. https://doi.org/10.1002/jctb.4257.

[17] S.E. Urbance, A.L. Pometto, A.A. DiSpirito, Y. Denli, Evaluation of succinic acid continuous and repeat-batch biofilm fermentation by *Actinobacillus succinogenes* using plastic composite support bioreactors., Appl. Microbiol. Biotechnol. 65 (2004) 664–670. https://doi.org/10.1007/s00253-004-1634-2.

[18] M.C.M. van Loosdrecht, J. Lyklema, W. Norde, A.J.B. Zehnder, Bacterial adhesion: A physicochemical approach, Microb. Ecol. 17 (1989) 1–15. https://doi.org/10.1007/BF02025589.

[19] R. Patel, Biofilms and antimicrobial resistance, Clin. Orthop. Relat. Res. NA; (2005) 41–47. https://doi.org/10.1097/01.blo.0000175714.68624.74.

[20] S.C. Mokwatlo, M.E. Nchabeleng, H.G. Brink, W. Nicol, Impact of metabolite accumulation on the structure, viability and development of succinic acid–producing biofilms of Actinobacillus succinogenes, Appl. Microbiol. Biotechnol. 103 (2019) 6205–6215. https://doi.org/10.1007/s00253-019-09888-8.

[21] S.C. Mokwatlo, H.G. Brink, W. Nicol, Effect of shear on morphology, viability and metabolic activity of succinic acid-producing Actinobacillus succinogenes biofilms, Bioprocess Biosyst. Eng. (2020). https://doi.org/10.1007/s00449-020-02322-8.

[22] S.C. Mokwatlo, W. Nicol, Structure and cell viability analysis of Actinobacillus succinogenes biofilms as biocatalysts for succinic acid production, Biochem. Eng. J. 128 (2017) 134–140. https://doi.org/10.1016/j.bej.2017.09.013.

[23] M.C.M. Van Loosdrecht, D. Eikelboom, A. Gjatelma, A. Mulder, L. Tijhuis, J.J.

Heijnen, Biofilm structures, Water Sci. Technol. 32 (1995) 35–43. https://doi.org/10.1016/0273-1223(96)00005-4.

[24] M.C.M. van Loosdrecht, C. Picioreanu, J.J. Heijnen, A more unifying hypothesis for biofilm structures, FEMS Microbiol. Ecol. 24 (1997) 181–183. https://doi.org/10.1111/j.1574-6941.1997.tb00434.x.

[25] P.S. Stewart, A review of experimental measurements of effective diffusive permeabilities and effective diffusion coefficients in biofilms., Biotechnol. Bioeng. 59 (1998) 261–272. https://doi.org/10.1002/(SICI)1097-0290(19980805)59:3<261::AID-BIT1>3.0.CO;2-9.

[26] H.G. Brink, W. Nicol, Succinic Acid Production by Actinobacillus Succinogenes in Chemostat and Biofilm Cultures, Chem. Eng. Trans. 49 (2016) 613–618. https://doi.org/10.3303/CET1649103.

[27] G.M. Klecka, W.J. Maier, Kinetics of microbial growth on pentachlorophenol, Appl. Environ. Microbiol. 49 (1985) 46–53. https://doi.org/10.1128/aem.49.1.46-53.1985.

[28] C.D. Van Heerden, W. Nicol, Continuous succinic acid fermentation by *Actinobacillus succinogenes*, Biochem. Eng. J. 73 (2013) 5–11. https://doi.org/10.1016/j.bej.2013.01.015.

[29] J. Villadsen, J. Nielsen, G. Lidén, Bioreaction Engineering Principles, 3rd ed., Springer, New York, 2011. https://doi.org/10.1007/978-1-4419-9688-6.

[30] R.J. Hyndman, G. Athanasopoulos, Forecasting: principles and practice, OTexts,

Heathmont, 2018.

[31] R.K. Hinson, W.M. Kocher, Model for effective diffusivities in aerobic biofilms, J. Environ. Eng. 122 (1996) 1023–1030. https://doi.org/10.1061/(ASCE)0733-9372(1996)122:11(103).

[32] E.W. Thiele, Relation between Catalytic Activity and Size of Particle, Ind. Eng. Chem. 31 (1939) 916–920. https://doi.org/10.1021/ie50355a027.

[33] H. Scott Fogler, Elements of chemical reaction engineering, Prentice Hall, Upper Saddle River, NJ, 1987. https://doi.org/10.1016/0009-2509(87)80130-6.

[34] T.H. Chilton, A.P. Colburn, Mass Transfer (Absorption) Coefficients: Prediction from Data on Heat Transfer and Fluid Friction, Ind. Eng. Chem. 26 (1934) 1183–1187. https://doi.org/10.1021/ie50299a012.

[35] D. Celmer, J.A. Oleszkiewicz, N. Cicek, Impact of shear force on the biofilm structure and performance of a membrane biofilm reactor for tertiary hydrogen-driven denitrification of municipal wastewater, Water Res. 42 (2008) 3057–3065. https://doi.org/10.1016/j.watres.2008.02.031.

[36] I. Bechthold, K. Bretz, S. Kabasci, R. Kopitzky, A. Springer, Succinic Acid: A New Platform Chemical for Biobased Polymers from Renewable Resources, Chem. Eng. Technol. 31 (2008) 647–654. https://doi.org/10.1002/ceat.200800063.